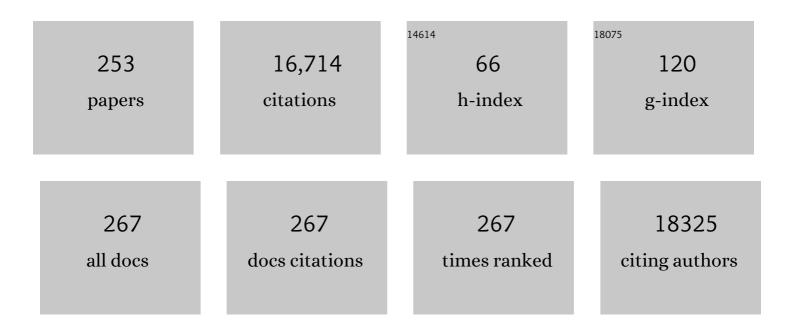


List of Publications by Year in descending order

Source: https://exaly.com/author-pdf/4534766/publications.pdf Version: 2024-02-01



7111/1/11

#	Article	IF	CITATIONS
1	Probing Defect Sites on CeO ₂ Nanocrystals with Well-Defined Surface Planes by Raman Spectroscopy and O ₂ Adsorption. Langmuir, 2010, 26, 16595-16606.	1.6	889
2	Role of Interfaces in Two-Dimensional Photocatalyst for Water Splitting. ACS Catalysis, 2018, 8, 2253-2276.	5.5	773
3	Anomalous High Ionic Conductivity of Nanoporous β-Li ₃ PS ₄ . Journal of the American Chemical Society, 2013, 135, 975-978.	6.6	709
4	On the structure dependence of CO oxidation over CeO2 nanocrystals with well-defined surface planes. Journal of Catalysis, 2012, 285, 61-73.	3.1	553
5	CO Oxidation on Supported Single Pt Atoms: Experimental and ab Initio Density Functional Studies of CO Interaction with Pt Atom on I-Al ₂ O ₃ (010) Surface. Journal of the American Chemical Society, 2013, 135, 12634-12645.	6.6	535
6	Introduction of π-Complexation into Porous Aromatic Framework for Highly Selective Adsorption of Ethylene over Ethane. Journal of the American Chemical Society, 2014, 136, 8654-8660.	6.6	383
7	Oneâ€5tep Synthesis of Nb ₂ O ₅ /C/Nb ₂ C (MXene) Composites and Their Use as Photocatalysts for Hydrogen Evolution. ChemSusChem, 2018, 11, 688-699.	3.6	315
8	2D/2D heterojunction of Ti ₃ C ₂ /g-C ₃ N ₄ nanosheets for enhanced photocatalytic hydrogen evolution. Nanoscale, 2019, 11, 8138-8149.	2.8	289
9	Nature of Active Sites and Surface Intermediates during SCR of NO with NH ₃ by Supported V ₂ O ₅ –WO ₃ /TiO ₂ Catalysts. Journal of the American Chemical Society, 2017, 139, 15624-15627.	6.6	266
10	A physical catalyst for the electrolysis of nitrogen to ammonia. Science Advances, 2018, 4, e1700336.	4.7	264
11	Vibrational spectra of alumina- and silica-supported vanadia revisited: An experimental and theoretical model catalyst study. Journal of Catalysis, 2004, 226, 88-100.	3.1	258
12	Titania Composites with 2 D Transition Metal Carbides as Photocatalysts for Hydrogen Production under Visible‣ight Irradiation. ChemSusChem, 2016, 9, 1490-1497.	3.6	253
13	High‣electivity Electrochemical Conversion of CO ₂ to Ethanol using a Copper Nanoparticle/Nâ€Doped Graphene Electrode. ChemistrySelect, 2016, 1, 6055-6061.	0.7	251
14	Thiolate Ligands as a Double-Edged Sword for CO Oxidation on CeO ₂ Supported Au ₂₅ (SCH ₂ CH ₂ Ph) ₁₈ Nanoclusters. Journal of the American Chemical Society, 2014, 136, 6111-6122.	6.6	245
15	Mesoporous MnCeOx solid solutions for low temperature and selective oxidation of hydrocarbons. Nature Communications, 2015, 6, 8446.	5.8	241
16	Understanding complete oxidation of methane on spinel oxides at a molecular level. Nature Communications, 2015, 6, 7798.	5.8	237
17	High-rate in-plane micro-supercapacitors scribed onto photo paper using in situ femtolaser-reduced graphene oxide/Au nanoparticle microelectrodes. Energy and Environmental Science, 2016, 9, 1458-1467.	15.6	202
18	Taming interfacial electronic properties of platinum nanoparticles on vacancy-abundant boron nitride nanosheets for enhanced catalysis. Nature Communications, 2017, 8, 15291.	5.8	200

#	Article	IF	CITATIONS
19	Imaging the Atomic Surface Structures of CeO ₂ Nanoparticles. Nano Letters, 2014, 14, 191-196.	4.5	183
20	Monolayer Ti ₃ C ₂ <i>T</i> _{<i>x</i>} as an Effective Co-catalyst for Enhanced Photocatalytic Hydrogen Production over TiO ₂ . ACS Applied Energy Materials, 2019, 2, 4640-4651.	2.5	177
21	In situ spectroscopy-guided engineering of rhodium single-atom catalysts for CO oxidation. Nature Communications, 2019, 10, 1330.	5.8	177
22	Shapeâ€Controlled Ceriaâ€based Nanostructures for Catalysis Applications. ChemSusChem, 2013, 6, 1821-1833.	3.6	176
23	Low temperature propane oxidation over Co3O4 based nano-array catalysts: Ni dopant effect, reaction mechanism and structural stability. Applied Catalysis B: Environmental, 2016, 180, 150-160.	10.8	174
24	On the Structure of Vanadium Oxide Supported on Aluminas:Â UV and Visible Raman Spectroscopy, UVâ^'Visible Diffuse Reflectance Spectroscopy, and Temperature-Programmed Reduction Studies. Journal of Physical Chemistry B, 2005, 109, 2793-2800.	1.2	167
25	Probing the Surface Sites of CeO ₂ Nanocrystals with Well-Defined Surface Planes via Methanol Adsorption and Desorption. ACS Catalysis, 2012, 2, 2224-2234.	5.5	165
26	Spectroscopic Investigation of Surface-Dependent Acid–Base Property of Ceria Nanoshapes. Journal of Physical Chemistry C, 2015, 119, 7340-7350.	1.5	156
27	Dibenzothiophene hydrodesulfurization activity and surface sites of silica-supported MoP, Ni2P, and NiMoP catalysts. Journal of Catalysis, 2004, 228, 298-310.	3.1	154
28	Highly selective adsorption of ethylene over ethane in a MOF featuring the combination of open metal site and π-complexation. Chemical Communications, 2015, 51, 2714-2717.	2.2	151
29	Direct Neutron Spectroscopy Observation of Cerium Hydride Species on a Cerium Oxide Catalyst. Journal of the American Chemical Society, 2017, 139, 9721-9727.	6.6	138
30	Influence of catalyst synthesis method on selective catalytic reduction (SCR) of NO by NH3 with V2O5-WO3/TiO2 catalysts. Applied Catalysis B: Environmental, 2016, 193, 141-150.	10.8	136
31	Fabrication of Au ₂₅ (SG) ₁₈ –ZIFâ€8 Nanocomposites: A Facile Strategy to Position Au ₂₅ (SG) ₁₈ Nanoclusters Inside and Outside ZIFâ€8. Advanced Materials, 2018, 30, 1704576.	11.1	129
32	Adsorption and Reaction of Acetaldehyde on Shape-Controlled CeO ₂ Nanocrystals: Elucidation of Structure–Function Relationships. ACS Catalysis, 2014, 4, 2437-2448.	5.5	128
33	Surface Reconstructions of Metal Oxides and the Consequences on Catalytic Chemistry. ACS Catalysis, 2019, 9, 5692-5707.	5.5	127
34	In-Plane Heterojunctions Enable Multiphasic Two-Dimensional (2D) MoS ₂ Nanosheets As Efficient Photocatalysts for Hydrogen Evolution from Water Reduction. ACS Catalysis, 2016, 6, 6723-6729.	5.5	116
35	Preparation and Characterization of PdFe Nanoleaves as Electrocatalysts for Oxygen Reduction Reaction. Chemistry of Materials, 2011, 23, 1570-1577.	3.2	106
36	Acid–base catalysis over perovskites: a review. Journal of Materials Chemistry A, 2018, 6, 2877-2894.	5.2	101

#	Article	IF	CITATIONS
37	The reaction route and active site of catalytic decomposition of hydrazine over molybdenum nitride catalyst. Journal of Catalysis, 2004, 224, 473-478.	3.1	100
38	Vacancy engineering of the nickel-based catalysts for enhanced CO2 methanation. Applied Catalysis B: Environmental, 2021, 282, 119561.	10.8	100
39	Adhesion and Atomic Structures of Gold on Ceria Nanostructures: The Role of Surface Structure and Oxidation State of Ceria Supports. Nano Letters, 2015, 15, 5375-5381.	4.5	98
40	Towards ALD thin film stabilized single-atom Pd ₁ catalysts. Nanoscale, 2016, 8, 15348-15356.	2.8	98
41	Oxidative Dehydrogenation of Propane to Propylene with Soft Oxidants via Heterogeneous Catalysis. ACS Catalysis, 2021, 11, 2182-2234.	5.5	97
42	Surface structure dependence of selective oxidation of ethanol on faceted CeO2 nanocrystals. Journal of Catalysis, 2013, 306, 164-176.	3.1	95
43	High-performance stacked in-plane supercapacitors and supercapacitor array fabricated by femtosecond laser 3D direct writing on polyimide sheets. Electrochimica Acta, 2017, 241, 153-161.	2.6	93
44	Synthesis of silica supported AuCu nanoparticle catalysts and the effects of pretreatment conditions for the CO oxidation reaction. Physical Chemistry Chemical Physics, 2011, 13, 2571.	1.3	92
45	Extraction, antioxidant and antibacterial activities of Broussonetia papyrifera fruits polysaccharides. International Journal of Biological Macromolecules, 2016, 92, 116-124.	3.6	92
46	In Situ Phase Separation of NiAu Alloy Nanoparticles for Preparing Highly Active Au/NiO CO Oxidation Catalysts. ChemPhysChem, 2008, 9, 2475-2479.	1.0	91
47	Structure of Vanadium Oxide Supported on Ceria by Multiwavelength Raman Spectroscopy. Journal of Physical Chemistry C, 2011, 115, 25368-25378.	1.5	91
48	Role Of CO ₂ As a Soft Oxidant For Dehydrogenation of Ethylbenzene to Styrene over a High-Surface-Area Ceria Catalyst. ACS Catalysis, 2015, 5, 6426-6435.	5.5	90
49	Diphosphine-Protected Au ₂₂ Nanoclusters on Oxide Supports Are Active for Gas-Phase Catalysis without Ligand Removal. Nano Letters, 2016, 16, 6560-6567.	4.5	88
50	Constructing Hierarchical Interfaces: TiO ₂ -Supported PtFe–FeO _{<i>x</i>} Nanowires for Room Temperature CO Oxidation. Journal of the American Chemical Society, 2015, 137, 10156-10159.	6.6	86
51	Photoinduced Strong Metal–Support Interaction for Enhanced Catalysis. Journal of the American Chemical Society, 2021, 143, 8521-8526.	6.6	85
52	Harnessing strong metal–support interactions via a reverse route. Nature Communications, 2020, 11, 3042.	5.8	84
53	Radical Chemistry and Reaction Mechanisms of Propane Oxidative Dehydrogenation over Hexagonal Boron Nitride Catalysts. Angewandte Chemie - International Edition, 2020, 59, 8042-8046.	7.2	83
54	Acid–Base Reactivity of Perovskite Catalysts Probed via Conversion of 2-Propanol over Titanates and Zirconates. ACS Catalysis, 2017, 7, 4423-4434.	5.5	81

#	Article	IF	CITATIONS
55	Catalysis on Singly Dispersed Rh Atoms Anchored on an Inert Support. ACS Catalysis, 2018, 8, 110-121.	5.5	81
56	Multiwavelength Raman Spectroscopic Study of Silica-Supported Vanadium Oxide Catalysts. Journal of Physical Chemistry C, 2010, 114, 412-422.	1.5	80
57	DRIFTS-QMS Study of Room Temperature CO Oxidation on Au/SiO ₂ Catalyst: Nature and Role of Different Au Species. Journal of Physical Chemistry C, 2009, 113, 3726-3734.	1.5	79
58	Synergistic Effects of Water and SO ₂ on Degradation of MIL-125 in the Presence of Acid Gases. Journal of Physical Chemistry C, 2016, 120, 27230-27240.	1.5	79
59	Reaction Pathways and Kinetics for Selective Catalytic Reduction (SCR) of Acidic NO _{<i>x</i>} Emissions from Power Plants with NH ₃ . ACS Catalysis, 2017, 7, 8358-8361.	5.5	78
60	Effects of Surface Terminations of 2D Bi ₂ WO ₆ on Photocatalytic Hydrogen Evolution from Water Splitting. ACS Applied Materials & Interfaces, 2020, 12, 20067-20074.	4.0	78
61	Descriptors for Hydrogen Evolution on Single Atom Catalysts in Nitrogen-Doped Graphene. Journal of Physical Chemistry C, 2020, 124, 19571-19578.	1.5	75
62	Support Shape Effect in Metal Oxide Catalysis: Ceria-Nanoshape-Supported Vanadia Catalysts for Oxidative Dehydrogenation of Isobutane. Journal of Physical Chemistry Letters, 2012, 3, 1517-1522.	2.1	72
63	In Situ FT-IR Spectroscopic Studies of CO Adsorption on Fresh Mo2C/Al2O3Catalyst. Journal of Physical Chemistry B, 2003, 107, 7088-7094.	1.2	71
64	Robust Ag nanoplate ink for flexible electronics packaging. Nanoscale, 2015, 7, 7368-7377.	2.8	71
65	Metallic Hydrogen in Atomically Precise Gold Nanoclusters. Chemistry of Materials, 2017, 29, 4840-4847.	3.2	70
66	Discriminating the Role of Surface Hydride and Hydroxyl for Acetylene Semihydrogenation over Ceria through <i>In Situ</i> Neutron and Infrared Spectroscopy. ACS Catalysis, 2020, 10, 5278-5287.	5.5	70
67	Aminopolymer functionalization of boron nitride nanosheets for highly efficient capture of carbon dioxide. Journal of Materials Chemistry A, 2017, 5, 16241-16248.	5.2	67
68	An overview of photocatalysis facilitated by 2D heterojunctions. Nanotechnology, 2019, 30, 502002.	1.3	66
69	Quantitative Analysis of the Morphology of {101} and {001} Faceted Anatase TiO ₂ Nanocrystals and Its Implication on Photocatalytic Activity. Chemistry of Materials, 2017, 29, 5591-5604.	3.2	65
70	On the surface sites of MoP/SiO2 catalyst under sulfiding conditions: IR spectroscopy and catalytic reactivity studies. Journal of Catalysis, 2004, 222, 41-52.	3.1	64
71	Stronger-than-Pt hydrogen adsorption in a Au ₂₂ nanocluster for the hydrogen evolution reaction. Journal of Materials Chemistry A, 2018, 6, 7532-7537.	5.2	63
72	Oxygenâ€Functionalized Few‣ayer Graphene Sheets as Active Catalysts for Oxidative Dehydrogenation Reactions. ChemSusChem, 2013, 6, 840-846.	3.6	61

#	Article	IF	CITATIONS
73	Effect of Dopants on the Adsorption of Carbon Dioxide on Ceria Surfaces. ChemSusChem, 2015, 8, 3651-3660.	3.6	61
74	UV Raman spectroscopic studies of V/î,-Al2O3 catalysts in butane dehydrogenation. Journal of Catalysis, 2006, 237, 220-229.	3.1	60
75	Elucidation of the Reaction Mechanism for High-Temperature Water Gas Shift over an Industrial-Type Copper–Chromium–Iron Oxide Catalyst. Journal of the American Chemical Society, 2019, 141, 7990-7999.	6.6	60
76	Shape Effect Undermined by Surface Reconstruction: Ethanol Dehydrogenation over Shape-Controlled SrTiO ₃ Nanocrystals. ACS Catalysis, 2018, 8, 555-565.	5.5	59
77	Nature of Reactive Hydrogen for Ammonia Synthesis over a Ru/C12A7 Electride Catalyst. Journal of the American Chemical Society, 2020, 142, 7655-7667.	6.6	59
78	Enhanced visible light photocatalytic water reduction from a g-C3N4/SrTa2O6 heterojunction. Applied Catalysis B: Environmental, 2017, 217, 448-458.	10.8	58
79	Selective conversion of bio-derived ethanol to renewable BTX over Ga-ZSM-5. Green Chemistry, 2017, 19, 4344-4352.	4.6	57
80	CO oxidation on Au/FePO4 catalyst: Reaction pathways and nature of Au sites. Journal of Catalysis, 2009, 266, 98-105.	3.1	56
81	Title is missing!. Catalysis Letters, 2002, 79, 21-25.	1.4	55
82	Visible-light-driven Bi ₂ O ₃ /WO ₃ composites with enhanced photocatalytic activity. RSC Advances, 2015, 5, 91094-91102.	1.7	54
83	Raman Spectroscopic Study of V/Î,-Al2O3Catalysts:  Quantification of Surface Vanadia Species and Their Structure Reduced by Hydrogen. Journal of Physical Chemistry C, 2007, 111, 16460-16469.	1.5	53
84	Interface Engineering of Earth-Abundant Transition Metals Using Boron Nitride for Selective Electroreduction of CO ₂ . ACS Applied Materials & Interfaces, 2018, 10, 6694-6700.	4.0	52
85	Effects of Sodium and Tungsten Promoters on Mg ₆ MnO ₈ -Based Core–Shell Redox Catalysts for Chemical Looping—Oxidative Dehydrogenation of Ethane. ACS Catalysis, 2019, 9, 3174-3186.	5.5	52
86	Selective catalytic reduction of NO by NH3 with WO3-TiO2 catalysts: Influence of catalyst synthesis method. Applied Catalysis B: Environmental, 2016, 188, 123-133.	10.8	51
87	DMOF-1 as a Representative MOF for SO ₂ Adsorption in Both Humid and Dry Conditions. Journal of Physical Chemistry C, 2018, 122, 23493-23500.	1.5	51
88	FT-IR Spectroscopic Studies of Thiophene Adsorption and Reactions on Mo2N/γ-Al2O3 Catalysts. Journal of Physical Chemistry B, 2002, 106, 979-987.	1.2	50
89	Low-Temperature Solution-Phase Synthesis of NiAu Alloy Nanoparticles via Butyllithium Reduction: Influences of Synthesis Details and Application As the Precursor to Active Au-NiO/SiO ₂ Catalysts through Proper Pretreatment. Journal of Physical Chemistry C, 2009, 113, 5758-5765.	1.5	50
90	Ultra-thin PtFe-nanowires as durable electrocatalysts for fuel cells. Nanotechnology, 2011, 22, 015602.	1.3	50

#	Article	IF	CITATIONS
91	Origin of Active Oxygen in a Ternary CuO _{<i>x</i>} /Co ₃ O ₄ –CeO ₂ Catalyst for CO Oxidation. Journal of Physical Chemistry C, 2014, 118, 27870-27877.	1.5	50
92	Understanding the Impact of Surface Reconstruction of Perovskite Catalysts on CH ₄ Activation and Combustion. ACS Catalysis, 2018, 8, 10306-10315.	5.5	50
93	<i>In Situ</i> Strong Metal–Support Interaction (SMSI) Affects Catalytic Alcohol Conversion. ACS Catalysis, 2021, 11, 1938-1945.	5.5	50
94	Raman study of Fano interference in <i>p</i> â€ŧype doped silicon. Journal of Raman Spectroscopy, 2010, 41, 1759-1764.	1.2	49
95	Effect of Surface Structure of TiO ₂ Nanoparticles on CO ₂ Adsorption and SO ₂ Resistance. ACS Sustainable Chemistry and Engineering, 2017, 5, 9295-9306.	3.2	49
96	Heterometal Incorporation in Metal-Exchanged Zeolites Enables Low-Temperature Catalytic Activity of NO _{<i>x</i>} Reduction. Journal of Physical Chemistry C, 2012, 116, 23322-23331.	1.5	48
97	Effect of metal oxides modification on CO2 adsorption performance over mesoporous carbon. Microporous and Mesoporous Materials, 2017, 249, 34-41.	2.2	47
98	Controlling Reaction Selectivity through the Surface Termination of Perovskite Catalysts. Angewandte Chemie - International Edition, 2017, 56, 9820-9824.	7.2	47
99	All-solid-state supercapacitors from natural lignin-based composite film by laser direct writing. Applied Physics Letters, 2019, 115, .	1.5	46
100	Direct Visualization and Control of Atomic Mobility at {100} Surfaces of Ceria in the Environmental Transmission Electron Microscope. Nano Letters, 2017, 17, 7652-7658.	4.5	45
101	CO oxidation over ceria supported Au22 nanoclusters: Shape effect of the support. Chinese Chemical Letters, 2018, 29, 795-799.	4.8	45
102	First Principles Insight into H ₂ Activation and Hydride Species on TiO ₂ Surfaces. Journal of Physical Chemistry C, 2018, 122, 20323-20328.	1.5	44
103	Solar-driven efficient methane catalytic oxidation over epitaxial ZnO/La0.8Sr0.2CoO3 heterojunctions. Applied Catalysis B: Environmental, 2020, 265, 118469.	10.8	44
104	Investigation of the selective sites on graphitic carbons for oxidative dehydrogenation of isobutane. Journal of Catalysis, 2009, 267, 158-166.	3.1	42
105	CO oxidation on phosphate-supported Au catalysts: Effect of support reducibility on surface reactions. Journal of Catalysis, 2011, 278, 133-142.	3.1	42
106	Impact of Surface Composition of SrTiO ₃ Catalysts for Oxidative Coupling of Methane. ChemCatChem, 2019, 11, 2107-2117.	1.8	41
107	Surface engineering of MXenes for energy and environmental applications. Journal of Materials Chemistry A, 2022, 10, 10265-10296.	5.2	41
108	A Raman Spectroscopic Study of the Speciation of Vanadia Supported on Ceria Nanocrystals with Defined Surface Planes. ChemCatChem, 2012, 4, 1653-1661.	1.8	40

#	Article	IF	CITATIONS
109	Toward the Design of a Hierarchical Perovskite Support: Ultra-Sintering-Resistant Gold Nanocatalysts for CO Oxidation. ACS Catalysis, 2017, 7, 3388-3393.	5.5	40
110	Ultrathin platinum nanowire based electrodes for high-efficiency hydrogen generation in practical electrolyzer cells. Chemical Engineering Journal, 2021, 410, 128333.	6.6	40
111	A review of the interactions between ceria and H2 and the applications to selective hydrogenation of alkynes. Chinese Journal of Catalysis, 2020, 41, 901-914.	6.9	40
112	Weak Sharp Solutions of Variational Inequalities in Hilbert Spaces. SIAM Journal on Optimization, 2004, 14, 1011-1027.	1.2	38
113	Effects of TiO ₂ in Low Temperature Propylene Epoxidation Using Gold Catalysts. Journal of Physical Chemistry C, 2018, 122, 1688-1698.	1.5	37
114	New Bonding Model of Radical Adsorbate on Lattice Oxygen of Perovskites. Journal of Physical Chemistry Letters, 2018, 9, 6321-6325.	2.1	37
115	Influence of absorption on quantitative analysis in Raman spectroscopy. Catalysis Today, 2006, 113, 40-47.	2.2	36
116	PdPt-TiO2 nanowires: correlating composition, electronic effects and O-vacancies with activities towards water splitting and oxygen reduction. Applied Catalysis B: Environmental, 2020, 277, 119177.	10.8	36
117	A Review on the Impact of SO ₂ on the Oxidation of NO, Hydrocarbons, and CO in Diesel Emission Control Catalysis. ACS Catalysis, 2021, 11, 12446-12468.	5.5	36
118	The role of surface vanadia species in butane dehydrogenation over VOx/Al2O3. Catalysis Today, 2009, 142, 143-151.	2.2	35
119	In situ studies of surface of NiFe2O4 catalyst during complete oxidation of methane. Surface Science, 2016, 648, 156-162.	0.8	35
120	A tailored multi-functional catalyst for ultra-efficient styrene production under a cyclic redox scheme. Nature Communications, 2021, 12, 1329.	5.8	35
121	Exploring perovskites for methane activation from first principles. Catalysis Science and Technology, 2018, 8, 702-709.	2.1	35
122	An IR Study on Selective Hydrogenation of 1,3-Butadiene on Transition Metal Nitrides:Â 1,3-Butadiene and 1-Butene Adsorption on Mo2N/I ³ -Al2O3Catalyst. Journal of Physical Chemistry B, 2000, 104, 12275-12281.	1.2	34
123	An IR study on the surface passivation of Mo2C/Al2O3 catalyst with O2, H2O and CO2. Physical Chemistry Chemical Physics, 2004, 6, 5603.	1.3	33
124	The synergic effect between Mo species and acid sites in Mo/HMCM-22 catalysts for methane aromatization. Physical Chemistry Chemical Physics, 2005, 7, 3102.	1.3	33
125	High Internal Quantum Efficiency of Nonpolar <i>a</i> -Plane AlGaN-Based Multiple Quantum Wells Grown on <i>r</i> -Plane Sapphire Substrate. ACS Photonics, 2018, 5, 1903-1906.	3.2	33
126	MoS2 nanosheet integrated electrodes with engineered 1T-2H phases and defects for efficient hydrogen production in practical PEM electrolysis. Applied Catalysis B: Environmental, 2022, 313, 121458.	10.8	33

#	Article	IF	CITATIONS
127	Solvent-free and one-pot synthesis of ultramicroporous carbons with ultrahigh nitrogen contents for sulfur dioxide capture. Chemical Engineering Journal, 2020, 391, 123579.	6.6	32
128	Engineering Porous Organic Cage Crystals with Increased Acid Gas Resistance. Chemistry - A European Journal, 2016, 22, 10743-10747.	1.7	31
129	Kinetics and Mechanism of Methanol Conversion over Anatase Titania Nanoshapes. ACS Catalysis, 2017, 7, 5345-5356.	5.5	31
130	A new trick for an old support: Stabilizing gold single atoms on LaFeO3 perovskite. Applied Catalysis B: Environmental, 2020, 261, 118178.	10.8	31
131	Perovskite-supported Pt single atoms for methane activation. Journal of Materials Chemistry A, 2020, 8, 4362-4368.	5.2	31
132	Pd-promoted WO3-ZrO2 for low temperature NOx storage. Applied Catalysis B: Environmental, 2020, 264, 118499.	10.8	30
133	A Principle for Highly Active Metal Oxide Catalysts via NaCl-Based Solid Solution. CheM, 2020, 6, 1723-1741.	5.8	30
134	Oxygen-assisted reduction of Au species on Au/SiO2 catalyst in room temperature CO oxidation. Chemical Communications, 2008, , 3308.	2.2	29
135	Role of defects and metal coordination on adsorption of acid gases in MOFs and metal oxides: An in situ IR spectroscopic study. Microporous and Mesoporous Materials, 2016, 227, 65-75.	2.2	29
136	Neutron Scattering Investigations of Hydride Species in Heterogeneous Catalysis. ChemSusChem, 2019, 12, 93-103.	3.6	29
137	Threeâ€Phase Catalytic System of H ₂ 0, Ionic Liquid, and VOPO ₄ –SiO ₂ Solid Acid for Conversion of Fructose to 5â€Hydroxymethylfurfural. ChemSusChem, 2014, 7, 1703-1709.	3.6	28
138	Carbon Monoxide Adsorption on Molybdenum Phosphides:Â Fourier Transform Infrared Spectroscopic and Density Functional Theory Studies. Journal of Physical Chemistry B, 2003, 107, 13698-13702.	1.2	26
139	Surface Structure Dependence of SO ₂ Interaction with Ceria Nanocrystals with Well-Defined Surface Facets. Journal of Physical Chemistry C, 2015, 119, 28895-28905.	1.5	26
140	Fundamental Understanding of the Interaction of Acid Gases with CeO ₂ : From Surface Science to Practical Catalysis. Industrial & Engineering Chemistry Research, 2016, 55, 3909-3919.	1.8	26
141	Defects reduction in a-plane AlGaN epi-layers grown on r-plane sapphire substrates by metal organic chemical vapor deposition. Applied Physics Express, 2017, 10, 011002.	1.1	25
142	Construction of 2D BiVO ₄ â^'CdSâ^'Ti ₃ C ₂ T _x Heterostructures for Enhanced Photoâ€redox Activities. ChemCatChem, 2020, 12, 3496-3503.	1.8	25
143	Defect Engineering of Ceria Nanocrystals for Enhanced Catalysis via a High-Entropy Oxide Strategy. ACS Central Science, 2022, 8, 1081-1090.	5.3	25
144	Growth and Electrochemical Characterization of Carbon Nanospike Thin Film Electrodes. Journal of the Electrochemical Society, 2014, 161, H558-H563.	1.3	24

#	Article	IF	CITATIONS
145	New Insights into the Bulk and Surface Defect Structures of Ceria Nanocrystals from Neutron Scattering Study. Chemistry of Materials, 2021, 33, 3959-3970.	3.2	24
146	Isolated Metal Sites in Cu–Zn–Y/Beta for Direct and Selective Butene-Rich C ₃₊ Olefin Formation from Ethanol. ACS Catalysis, 2021, 11, 9885-9897.	5.5	24
147	Sulfur Effect on Mo2N/γ-Al2O3 Catalyst Studied by in Situ FT-IR Spectroscopy. Journal of Catalysis, 2000, 194, 23-32.	3.1	23
148	Low-Temperature Isomerization of 1-Butene on Mo2N/γ-Al2O3 Catalyst Studied by in Situ FT-IR Spectroscopy. Journal of Physical Chemistry B, 2001, 105, 9183-9190.	1.2	23
149	Deep Learning Accelerated Determination of Hydride Locations in Metal Nanoclusters. Angewandte Chemie - International Edition, 2021, 60, 12289-12292.	7.2	23
150	Self-Assembly of Metal Oxide Nanoparticles into Hierarchically Patterned Porous Architectures Using Ionic Liquid/Oil Emulsions. Langmuir, 2009, 25, 7229-7233.	1.6	22
151	Activation and surface reactions of CO and H2 on ZnO powders and nanoplates under CO hydrogenation reaction conditions. Journal of Energy Chemistry, 2020, 50, 351-357.	7.1	22
152	A comparison of catalyst deactivation of vanadia catalysts used for alkane dehydrogenation. Chemical Engineering Journal, 2006, 120, 127-132.	6.6	21
153	Interaction of SO ₂ with ZnO Nanoshapes: Impact of Surface Polarity. Journal of Physical Chemistry C, 2019, 123, 11772-11780.	1.5	21
154	Elucidating the origin of selective dehydrogenation of propane on Î ³ -alumina under H2S treatment and co-feed. Journal of Catalysis, 2021, 394, 142-156.	3.1	21
155	Inelastic Neutron Scattering Observation of Plasma-Promoted Nitrogen Reduction Intermediates on Ni/γ-Al ₂ O ₃ . ACS Energy Letters, 2021, 6, 2048-2053.	8.8	20
156	Multiple Promotional Effects of Vanadium Oxide on Boron Nitride for Oxidative Dehydrogenation of Propane. Jacs Au, 2022, 2, 1096-1104.	3.6	20
157	<i>In Situ</i> High Temperature Surface Enhanced Raman Spectroscopy for the Study of Interface Phenomena: Probing a Solid Acid on Alumina. Journal of Physical Chemistry C, 2011, 115, 9068-9073.	1.5	19
158	Galvanic synthesis of bi-modal porous metal nanostructures using aluminum nanoparticle templates. Materials Letters, 2012, 88, 143-147.	1.3	19
159	Single Pd Atoms on Î,-Al2O3 (010) Surface do not Catalyze NO Oxidation. Scientific Reports, 2017, 7, 560.	1.6	19
160	Controlling Reaction Selectivity through the Surface Termination of Perovskite Catalysts. Angewandte Chemie, 2017, 129, 9952-9956.	1.6	19
161	Molecular structure and sour gas surface chemistry of supported K2O/WO3/Al2O3 catalysts. Applied Catalysis B: Environmental, 2018, 232, 146-154.	10.8	19
162	Fabrication of a Pillared ZSM-5 Framework for Shape Selectivity of Ethane Dehydroaromatization. Industrial & Engineering Chemistry Research, 2019, 58, 7094-7106.	1.8	19

#	Article	IF	CITATIONS
163	The interplay between surface facet and reconstruction on isopropanol conversion over SrTiO3 nanocrystals. Journal of Catalysis, 2020, 384, 49-60.	3.1	19
164	Measuring and directing charge transfer in heterogenous catalysts. Nature Communications, 2022, 13,	5.8	19
165	In situ growth synthesis of heterostructured LnPO4–SiO2 (Ln = La, Ce, and Eu) mesoporous materials as supports for small gold particles used in catalytic CO oxidation. Journal of Materials Chemistry, 2012, 22, 25227.	6.7	18
166	Aromatic–hydroxyl interaction of an alpha-aryl ether lignin model-compound on SBA-15, present at pyrolysis temperatures. Physical Chemistry Chemical Physics, 2014, 16, 24188-24193.	1.3	18
167	Alcohol-Induced Low-Temperature Blockage of Supported-Metal Catalysts for Enhanced Catalysis. ACS Catalysis, 2020, 10, 8515-8523.	5.5	18
168	Hydrogen in Nanocatalysis. Journal of Physical Chemistry Letters, 2020, 11, 7049-7057.	2.1	18
169	Oxidative dehydrogenation of isobutane over vanadia catalysts supported by titania nanoshapes. Catalysis Today, 2016, 263, 84-90.	2.2	17
170	Defect-Regulated Frustrated-Lewis-Pair Behavior of Boron Nitride in Ambient Pressure Hydrogen Activation. Journal of the American Chemical Society, 2022, 144, 10688-10693.	6.6	17
171	Characterization of weakly sharp solutions of a variational inequality by its primal gap function. Optimization Letters, 2016, 10, 563-576.	0.9	16
172	Understanding the conversion of ethanol to propene on In2O3 from first principles. Catalysis Today, 2020, 350, 19-24.	2.2	16
173	All-solid-state Z-scheme BiVO4â^'Bi6O6(OH)3(NO3)3 heterostructure with prolonging electron-hole lifetime for enhanced photocatalytic hydrogen and oxygen evolution. Journal of Materials Science and Technology, 2021, 77, 117-125.	5.6	16
174	Manipulating Copper Dispersion on Ceria for Enhanced Catalysis: A Nanocrystalâ€Based Atomâ€Trapping Strategy. Advanced Science, 2022, 9, e2104749.	5.6	16
175	Effects of Si-doping on structural and electrical characteristics of polar, semi-polar, and non-polar AlGaN epi-layers. Materials Science in Semiconductor Processing, 2016, 42, 344-348.	1.9	15
176	Controlling interfacial properties in supported metal oxide catalysts through metal–organic framework templating. Journal of Materials Chemistry A, 2017, 5, 13565-13572.	5.2	15
177	Catalytic Dehydration of Biomass Derived 1-Propanol to Propene over M-ZSM-5 (M = H, V, Cu, or Zn). Industrial & Engineering Chemistry Research, 2017, 56, 4302-4308.	1.8	15
178	Inelastic neutron scattering, Raman and DFT investigations of the adsorption of phenanthrenequinone on onion-like carbon. Carbon, 2013, 52, 150-157.	5.4	14
179	Elucidating the Mechanism of Ambient-Temperature Aldol Condensation of Acetaldehyde on Ceria. ACS Catalysis, 2021, 11, 8621-8634.	5.5	14
180	A novel reaction on a Mo2N/γ-Al2O3 catalyst: low-temperature isomerization of but-1-ene. Chemical Communications, 2001, , 701-702.	2.2	13

#	Article	IF	CITATIONS
181	Effects of Si-doping on structural, electrical, and optical properties of polar and non-polar AlGaN epi-layers. Superlattices and Microstructures, 2016, 96, 1-7.	1.4	13
182	Promoting Pt catalysis for CO oxidation <i>via</i> the Mott–Schottky effect. Nanoscale, 2019, 11, 18568-18574.	2.8	13
183	Machine Learning Method Reveals Hidden Strong Metalâ€&upport Interaction in Microscopy Datasets. Small Methods, 2021, 5, 2100035.	4.6	13
184	Multi-wavelength Raman spectroscopy study of supported vanadia catalysts: Structure identification and quantification. Chinese Journal of Catalysis, 2014, 35, 1591-1608.	6.9	12
185	In situ spectroscopic insights into the redox and acid-base properties of ceria catalysts. Chinese Journal of Catalysis, 2021, 42, 2122-2140.	6.9	12
186	Title is missing!. Catalysis Surveys From Asia, 2003, 7, 103-119.	1.0	11
187	Radical Chemistry and Reaction Mechanisms of Propane Oxidative Dehydrogenation over Hexagonal Boron Nitride Catalysts. Angewandte Chemie, 2020, 132, 8119-8123.	1.6	11
188	On the Structural Transformation of Ni/BaH2 During a N2-H2 Chemical Looping Process for Ammonia Synthesis: A Joint In Situ Inelastic Neutron Scattering and First-Principles Simulation Study. Topics in Catalysis, 2021, 64, 685-692.	1.3	11
189	Epoxidation of cyclohexene on Ti/SiO2 catalysts prepared by chemical grafting TiCl4 on deboronated silica xerogel. Journal of Molecular Catalysis A, 2001, 172, 219-225.	4.8	10
190	Adsorption and reaction of thiophene and H2S on Mo2C/Al2O3 catalyst studied by in situ FT-IR spectroscopy. Physical Chemistry Chemical Physics, 2004, 6, 5596.	1.3	10
191	Promotional Effects of In on Non-Oxidative Methane Transformation Over Mo-ZSM-5. Catalysis Letters, 2016, 146, 1903-1909.	1.4	10
192	High hole concentration in nonpolar a-plane p-AlGaN films with Mg-delta doping technique. Superlattices and Microstructures, 2017, 109, 880-885.	1.4	10
193	Enhanced hole concentration and improved surface morphology for nonpolar a-plane p-type AlGaN/GaN superlattices grown with indium-surfactant. Superlattices and Microstructures, 2019, 130, 396-400.	1.4	10
194	Optimizing the structural configuration of FePt-FeOx nanoparticles at the atomic scale by tuning the post-synthetic conditions. Nano Energy, 2019, 55, 441-446.	8.2	10
195	Cu-Enhanced Surface Defects and Lattice Mobility of Pr-CeO ₂ Mixed Oxides. Journal of Physical Chemistry C, 2016, 120, 27996-28008.	1.5	9
196	Ab Initio Density Functional Calculations and Infra-Red Study of CO Interaction with Pd Atoms on Î _s -Al2O3 (010) Surface. Scientific Reports, 2017, 7, 6231.	1.6	9
197	Indium-surfactant-assisted epitaxial growth of semi-polar \$\$left(11overline{2}2ight)\$\$ 11 2 Â⁻ 2 plane Al0.42Ga0.58N films. Journal of Materials Science: Materials in Electronics, 2017, 28, 15217-15223.	1.1	9
198	Effects of indium surfactant on growth and characteristics of Â(112Â ⁻ 2) plane AlGaN-based multiple quantum wells. Optical Materials Express, 2018, 8, 24.	1.6	9

#	Article	IF	CITATIONS
199	Popularity-Based and Version-Aware Caching Scheme at Edge Servers for Multi-Version VoD Systems. IEEE Transactions on Circuits and Systems for Video Technology, 2021, 31, 1234-1248.	5.6	9
200	Mechanistic Understanding of Catalytic Conversion of Ethanol to 1-Butene over 2D-Pillared MFI Zeolite. Journal of Physical Chemistry C, 2020, 124, 28437-28447.	1.5	9
201	Manganese Catalyzed Partial Oxidation of Light Alkanes. ACS Catalysis, 2022, 12, 5356-5370.	5.5	9
202	Epitaxial growth of semiâ€polar (11â€22) plane AlGaN epiâ€layers on mâ€plane (10â€10) sapphire substrates. Physica Status Solidi (A) Applications and Materials Science, 2017, 214, 1600802.	0.8	8
203	Influence of nitridation process on characteristics of N-polar AlGaN films grown by MOCVD. Materials Science in Semiconductor Processing, 2017, 64, 147-151.	1.9	8
204	Characterizations of weakly sharp solutions for a variational inequality with a pseudomonotone mapping. European Journal of Operational Research, 2018, 265, 448-453.	3.5	8
205	Acetic Acid/Propionic Acid Conversion on Metal Doped Molybdenum Carbide Catalyst Beads for Catalytic Hot Gas Filtration. Catalysts, 2018, 8, 643.	1.6	8
206	Study of dual nitridation processes in growth of non-polar a-plane AlGaN epi-layers. Materials Letters, 2018, 227, 108-111.	1.3	8
207	Atomically Dispersed Tin-Modified \hat{I}^3 -alumina for Selective Propane Dehydrogenation under H ₂ S Co-feed. ACS Catalysis, 2021, 11, 13472-13482.	5.5	8
208	Can Li: A Career in Catalysis. ACS Catalysis, 2022, 12, 3063-3082.	5.5	8
209	Gâteaux differentiability of the dual gap function of a variational inequality. European Journal of Operational Research, 2008, 190, 328-344.	3.5	7
210	Study of NH3 flow duty-ratio in pulsed-flow epitaxial growth of non-polar a-plane Al0.34Ga0.66N films. Materials Science in Semiconductor Processing, 2019, 90, 219-224.	1.9	7
211	CO ₂ methanation reaction pathways over unpromoted and NaNO ₃ -promoted Ru/Al ₂ O ₃ catalysts. Catalysis Science and Technology, 2022, 12, 4637-4652. Effects of Mg-doping on characteristics of semi-polar <mml:math< td=""><td>2.1</td><td>7</td></mml:math<>	2.1	7
212	xmlns:mml="http://www.w3.org/1998/Math/MathML" altimg="si1.gif" overflow="scroll"> <mml:mrow><mml:mo< td=""><td></td><td></td></mml:mo<></mml:mrow>		

#	Article	IF	CITATIONS
217	The Characterization and Structure-Dependent Catalysis of Ceria with Well-Defined Facets. , 2015, , 71-97.		5
218	Epitaxial growth and characterization of nonpolar <i>a</i> -plane AlGaN films with MgN/AlGaN insertion layers. Applied Physics Express, 2017, 10, 045503.	1.1	5
219	Improved crystalline quality of N-polar GaN epitaxial layers grown with reformed flow-rate-modulation technology. Japanese Journal of Applied Physics, 2017, 56, 015501.	0.8	5
220	Enhanced hole concentration in nonpolara-plane p-AlGaN film with multiple-step rapid thermal annealing technique. Journal Physics D: Applied Physics, 2018, 51, 095101.	1.3	5
221	Stable Surface Terminations of a Perovskite Oxyhydride from First-Principles. Journal of Physical Chemistry C, 2020, 124, 18557-18563.	1.5	5
222	Revealing the interplay between "intelligent behavior―and surface reconstruction of non-precious metal doped SrTiO3 catalysts during methane combustion. Catalysis Today, 2022, , .	2.2	5
223	Sulfur effect on Mo2 N/λ-Al2O3 catalyst studied by in situ FT-IR spectroscopy. Studies in Surface Science and Catalysis, 2000, 130, 2819-2824.	1.5	4
224	Effects of growth temperature on characteristics of Mg-delta-doped p-AlInGaN epi-layers. Superlattices and Microstructures, 2016, 98, 181-186.	1.4	4
225	World Trade Wars: Scenario Calculations of Consequences. Herald of the Russian Academy of Sciences, 2020, 90, 88-97.	0.2	4
226	Ammonia synthesis on BaTiO _{2.5} H _{0.5} : computational insights into the role of hydrides. Physical Chemistry Chemical Physics, 2022, 24, 1496-1502.	1.3	4
227	The convexity of the solution set of a pseudoconvex inequality. Nonlinear Analysis: Theory, Methods & Applications, 2008, 69, 1666-1674.	0.6	3
228	Crucial influential factor on background electron concentration in semi-polar (11 <mml:math) 0="" etqq0="" rgb<="" td="" tj=""><td>T /Overlock 1.4</td><td>2 10 Tf 50 317 3</td></mml:math)>	T /Overlock 1.4	2 10 Tf 50 317 3
	plane AlGaN epi-layers. Superlattices and Microstructures, 2019, 125, 338-342.		
229	Effect of Hydrogen-Induced Metallization on Chemisorption. Journal of Physical Chemistry C, 2019, 123, 15171-15175.	1.5	3
230	H ₂ O-prompted CO ₂ capture on metal silicates <i>in situ</i> generated from SBA-15. RSC Advances, 2020, 10, 28731-28740.	1.7	3
231	Selective Hydrogenation of 1,3-Butadiene on Molybdenum Nitride Catalyst: Identification of the Adsorbed Hydrocarbonaceous Species. Studies in Surface Science and Catalysis, 2001, 138, 445-452.	1.5	2
232	Resonance Raman Spectroscopy -Î [~] -Al2O3-Supported Vanadium Oxide Catalysts as an Illustrative Example. , 0, , 177-194.		2
233	Reply to Comment on "Multiwavelength Raman Spectroscopic Study of Silica-Supported Vanadium Oxide Catalystsâ€, Journal of Physical Chemistry C, 2011, 115, 10925-10928.	1.5	2
234	Application Analysis on Large-Scale Computation for Social and Economic Systems: Application Case		2

from China. , 2015, , .

#	Article	IF	CITATIONS
235	Understanding Methanol Coupling on SrTiO3 from First Principles. Journal of Physical Chemistry C, 2018, 122, 7210-7216.	1.5	2
236	Oxygenâ€Functionalized Few‣ayer Graphene Sheets as Active Catalysts for Oxidative Dehydrogenation Reactions. ChemSusChem, 2013, 6, 732-732.	3.6	1
237	The impact of purging on the quality of AlGaN/GaN multiple quantum wells grown on AlN/sapphire template. Journal of Physics: Conference Series, 2017, 844, 012015.	0.3	1
238	Improvement of properties in nonpolar a-plane p-AlGaN films by Mg-delta doping method. , 2017, , .		1
239	Epitaxial growth and characterization of non-polar <i>a</i> -plane AlGaN films with MgN/AlGaN insertion layers. Journal of Physics: Conference Series, 2017, 844, 012003.	0.3	1
240	Work-in-Progress: Version-Aware Video Caching Strategy for Multi-version VoD Systems. , 2019, , .		1
241	Preface to Special Issue on Neutron Scattering for Catalysis. Topics in Catalysis, 2021, 64, 591-592.	1.3	1
242	In situ IR Spectroscopic Studies on Molybdenum Nitride Catalysts: Active Sites and Surface Reactions. ChemInform, 2004, 35, no.	0.1	0
243	A Region-Interactive Retrieval Model Based on IRM Algorithm. , 0, , .		0
244	Utilizing Surface Enhanced Raman Spectroscopy for the Study of Interfacial Phenomena: Probing Interactions on an Alumina Surface. ACS Symposium Series, 2013, , 101-114.	0.5	0
245	Infrared Spectroscopic Insights into the Role of the Support in Heterogeneous Gold Catalysis. RSC Catalysis Series, 2014, , 512-532.	0.1	0
246	Atomic Surface Structures of Oxide Nanoparticles with Well-defined Shapes. Microscopy and Microanalysis, 2016, 22, 360-361.	0.2	0
247	Improvement of properties for nonpolar a-plane p-AlGaN with Mg-delta doping technique. , 2017, , .		0
248	An extend RBAC model for privacy protection in HIS. , 2018, , .		0
249	Neutron Scattering Investigations of Hydride Species in Heterogeneous Catalysis. ChemSusChem, 2019, 12, 5-5.	3.6	0
250	Titelbild: Radical Chemistry and Reaction Mechanisms of Propane Oxidative Dehydrogenation over Hexagonal Boron Nitride Catalysts (Angew. Chem. 21/2020). Angewandte Chemie, 2020, 132, 8045-8045.	1.6	0
251	Deep Learning Accelerated Determination of Hydride Locations in Metal Nanoclusters. Angewandte Chemie, 2021, 133, 12397-12400.	1.6	0
252	Implementation and Analysis of Hybrid DRAM PUFs on FPGA. , 2021, , .		0

#	Article	IF	CITATIONS
	Enhanced performance of (<mml:math)="" 0.78<="" 1="" etqq1="" td="" tj="" xmlns:mml="http://www.w3.org/1998/Math/MathML"><td>4314 rgBT</td><td>/Overlock 10</td></mml:math>	4314 rgBT	/Overlock 10
253		1.3	Ο
	with indium surfactant. Materials Letters, 2022, 324, 132675.		